RESEARCH ARTICLE

In vitro toxicity assessment of uranium particulates on different human lung epithelial cell models

Shepard C. Moore, Laura M. Lilley[¤a‡], Julie Strickland[¤b‡], Mohammad Omar Ishak[‡], William Conor Emberley[¤c‡], Brian L. Scott[‡], Gregory L. Wagner[‡], Warren J. Oldham[‡], Murray E. Moore[‡], Harshini Mukundan[¤d], Jennifer Foster Harris*

Los Alamos National Laboratory, Los Alamos, New Mexico, United States of America

◉ These authors contributed equally to this work.
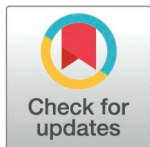‡ LML, JS, MOI, WCE, BLS, GLW, WJO and MEM also contributed equally to this work.
¤a Current address: TerraPower LLC, Bellevue, Washington, United States of America
¤b Current address: Lovelace Biomedical Research Institute, Albuquerque, New Mexico, United States of America
¤c Current address: Washington State Department of Agriculture, Olympia, Washington, United States of America
¤d Current address: Lawrence Berkeley Laboratory, Berkeley, California, United States of America
* jfharris@lanl.gov

Abstract

Inhalation of uranium aerosols produced via human activities such as mining can pose a threat to human respiratory systems. Uranium oxide particulates emit short-range alpha particles that elicit DNA and direct damage, beyond associated physiochemical heavy-metal toxicity, to internal epithelial tissues. The availability of reliable *in vitro* models to study radiation exposure can greatly enhance our ability to understand and combat the biological impacts of exposure. However, the toxicological effects of alpha emissions and/or the oxidation states of uranium particulates vary across different human lung epithelial cell models and have not been systematically compared. We have endeavored to address this limitation by comparing impacts in three different human lung cell models: primary human bronchial and tracheal epithelial cells, primary human small airway epithelial cells, and human adenocarcinoma alveolar basal epithelial cells. Other studies have mainly investigated the toxicity of depleted uranium. Here, we compared the exposure of uranium oxide particulates (U_3O_8 and UO_3) of different enrichment states on the chosen cell systems. Each cell model was exposed to 0.1, 1, 10, 50, 100, and 500 µg/mL of depleted U_3O_8, highly-enriched U_3O_8, and natural UO_3 particulates for 24 hours in submerged monolayer cultures. We compared viability and superoxide dismutase activity results across cell lines and uranium enrichment/ oxidative states. The results showed that 1) the oxide state of the particulates affected cell viability, implying that uranium's different oxidation states contribute to different toxicological responses, and 2) each cell model reacts differently when exposed to uranium oxides, which may provide insights

into the mechanistic processes associated with the exposure of radiological particulates on different biological systems. For instance, increased uranium enrichment corresponds to increased toxicity for the primary cells, but not for the immortalized cells. Our study shows that a holistic approach that incorporates similarities between model systems and types of radionuclides is required to truly develop empirical solutions for radiation exposure.

Introduction

Acute and chronic exposure to inhaled alpha (α)-emitting radioactive particulates, like uranium (U), from environmental, occupational, and enriched sources may lead to health risks to the human respiratory system due to its chemical and radiological toxicity [1–5]. Studies indicate that the epithelial lining of the lungs is the most susceptible area to internalized ionizing radiation, especially α-emissions [6]. Alpha particles cause cellular damage by directly breaking DNA strands, disrupting cell homeostasis, destroying cell membranes; and by indirectly generating reactive oxygen/nitrogen species to ravage cell integrity [7–15].

Uranium is a common heavy metal found in the earth's crust. There are three naturally occurring isotopes U-238 ($t_{1/2}$ = 4.46x10^9 y), U-235 ($t_{1/2}$ = 7.04x10^8 y), and U-234 ($t_{1/2}$ = 2.46x10^5 y) all producing α-particles [16]. Uranium is extracted from mines, used as fuel in nuclear power plants, found in groundwater via soil, and is a parent of many radioisotopes for medical, industrial, and military defense purposes [17]. Uranium has a tunable isotopic ratio, meaning that it is possible to vary the amount of general radioactivity—for the work in this manuscript, specifically α-emissions—in each sample to depleted (DU), natural (NatU), or highly enriched (HEU) values by decreasing or increasing the amount of its most fissile isotope, U-235 [18]. DU is a byproduct of the production of HEU and is used for many military munitions, radiation shielding, nuclear power plants, and nuclear weapons [19]. NatU, derived from uranium mining, can be deposited in soil, rock, and water, which can consequently leach into human infrastructure. One of the primary properties of NatU is its potential to be enriched to HEU or DU [20]. HEU is typically used for nuclear power, nuclear weapons, naval propulsion, and research reactors [21,22]. Whereas each of these uranium enrichment states can elicit negative health effects in human lung epithelial cells, the correlation between cellular toxicity and enrichment remains poorly understood [23].

The oxidation state of the uranium can vary, influencing associated biological effects on living systems. The common oxidation state(s) of uranium are at U(IV) and U(VI), for example, uranium dioxide (UO_2) and uranium trioxide (UO_3), respectively [24]. A mixed valence configuration is possible for triuranium octoxide (U_3O_8) that has potential combinations of U(IV), U(V), and U(VI) states [25]. The different oxidative states vary with regard to thermostability and reactivity as well. Uranium is usually shipped between facilities in its thermodynamically stable state, U_3O_8, and not as UO_2, which is relatively less stable and can undergo further oxidation in the presence of air or aqueous buffers to UO_3 or U_3O_8 [26].

The form of the isotope used in most toxicity studies exploring biological impact is dissolved uranium (e.g., uranium salts such as uranyl acetate) [27,28]. However, in one study, Harris et al. showed that 60% of inhaled uranium particulates were still present in the human body after 32 days of exposure, highlighting the urgent need to study insoluble uranium particulate species in a biological context [29]. U_3O_8 and UO_3 particulates have poor solubilities in water and are known to be retained within the lungs for several years, allowing for long-term exposure to the heavy metal and high-energy α-emissions [30–32]. Differences in sensitivity of upper or lower airways to radioactive particulates remain poorly studied [33,34]. *In vitro* toxicological (human) cell models provide a potential path to assess uranium particulate exposure effects [35]. However, the physiological relevance of these studies, translational value of the garnered information, and the variability in outcomes across various cell models remain poorly characterized and should be further explored.

Adenocarcinoma alveolar basal epithelial cells (A549), a human alveolar type II pulmonary epithelial cell, are often used as a lung surrogate due to their ease of cultivation, proliferation, and (almost) unlimited supply [36,37]. However, A549s are an immortalized cell line that is known to introduce unique artifacts into research results due to their chronic genetic drift [38–40]. Such genetic drift has potentially skewed toxicological interpretations of assumed toxicants due to A549's lowered sensitivity, as seen in tobacco smoke and lipopolysaccharide (LPS) [41–43]. Primary human lung cells, such as primary human bronchial and tracheal epithelial cells (HBTEC) and primary human small airway epithelial cells (HSAEC), may provide more physiologically relevant *in vitro* models [41]. Unlike immortalized A549s, primary cell lines have limited lifetimes, passage numbers, and unique genomic profiles from each donor, elevating the complexity and cost of experimentation [44]. Thus, an ideal *in vitro* model system for studying the impact of radiation does not exist, and further investigation is needed to characterize the tissues used in understanding the radiobiological effects of α-emitting materials on relevant human-specific respiratory systems [45–47].

The purpose of this study was to begin addressing the aforementioned limitations. We performed simultaneous comparative investigations of cytotoxic and mechanistic effects of increased enrichment and oxidation state of uranium particulates on several *in vitro* human epithelial lung cell models—HBTEC, HSAEC, and A549. We explore differences in upper and lower respiratory airway cells to radioactive particulates via comparison of toxicological response of upper (HBTEC), middle (HSAEC), and lower (A549) respiratory tract cells. We hypothesized that the most cellular cytotoxicity and damage will be evident with HEU, even at lower concentrations, because of significantly increased α-radiation activity. Other investigators have hypothesized that primary cell lines will be more susceptible to exposure because of their less robust nature compared to immortalized cell lines [48]. To evaluate this, we used multi-modal comprehensive analytics to characterize both the particulates and the biological outcomes.

Differences in susceptibility between cell models can inform on potential use cases for each model for future α-emitter radionuclide toxicity studies. Additionally, due to uranium's lower activity even when highly enriched, our findings may enable identification of a model system that can provide insight into the effects of other, more hazardous, α-emitters or heavy metals in the respiratory system.

Materials and methods

Uranium oxide particulates were synthesized and characterized to validate U-235 isotopic ratios (DU < 0.7%, NatU ≥ 0.7%, HEU > 20%), and diameters were respirable for humans according to the International Commission on Radiological Protection (ICRP) (<10 μm mass median aerodynamic diameter, MMAD) [49].

Uranium oxide synthesis

Each uranium oxide sample (DU U_3O_8, NatU UO_3, and HEU U_3O_8) was freshly prepared and purified to reduce impurities associated with aging of radiological materials and individually followed the subsequent synthesis procedure. A solid metal bar of uranium (DU 100 g, NatU 4 g, HEU 0.495 g) was dissolved in ~100 mL of Optima grade concentrated hydrochloric

acid (HCl, FisherSci, A466-500), with additional hydrogen peroxide (H_2O_2, FisherSci, P170-500) to speed up dissolution, in a round- bottom flask, producing uranyl (UO_2^{2+}). The dissolved metal was purified in accordance with Wilkerson et al. using a Reillex HPQ Polymer Ion Exchange column (Vertellus) with concentrated hydrochloric acid (HCl) and 0.01 M HCl as an eluent [50]. Once the purified uranium was collected, ammonium hydroxide (NH_4OH, FisherSci, A470-500) was added dropwise to reach a desired pH of 3.0, then H_2O_2 was added dropwise to produce the precipitate uranyl peroxide hydrate ($UO_2(O_2) \cdot xH_2O$) lowering the pH back to 1.0. The process was repeated by adjusting the pH to 3.0 with NH_4OH until the addition of H_2O_2 did not cause a decrease in pH. The yellow precipitate was then vacuum filtered through a fine glass frit, washed three times with ~30 mL of MilliQ water, and left to air-dry overnight. Once dry, the recovered uranium was crushed to a fine powder using a mortar and pestle, loaded in a platinum foil- lined ceramic boat, and then fired in a tube furnace at 800 °C for 20 hours in air, producing a black U_3O_8 powder [51,52]. The olive green natural UO_3 powder was produced the same way as depleted and highly enriched U_3O_8, except the firing time was increased to 40 hours. A diagram of the synthesis is shown in S1 Fig in S1 File.

Particulate preparation and characterization

Control particulates titanium dioxide (TiO_2, rutile powder, < 5 µm, > 99.9% trace metals basis, Lot# MKCG2282) and silicon dioxide (SiO_2, ~ 99%, 0.5 - 10 µm, approximately 80% between 1–5 µm, Lot# SLCH1152) were obtained from Sigma Aldrich. All U_3O_8 and UO_3 particulates were pushed through individual <25 µm sieves (Industrial Netting) with a fine paint brush in a chemical/radiological fume hood to closely achieve a target size of <10 µm MMAD. The sieved material was collected on aluminum foil underneath the sieve and carefully transferred to labeled glass scintillation vials for long-term storage.

Powder X-ray diffraction (p-XRD) analysis. All synthesized U_3O_8 and UO_3 samples were verified using powder X-ray diffraction (p-XRD) analysis (S2 Fig in S1 File) as described previously [50]. Briefly, powder patterns of samples at time 0 were collected on a Bruker D8 Discover diffractometer equipped with either a Hi-Star area detector or a high-resolution NiI scintillation detector and monochromatized Cu Kα X-rays. Qualitative analyses were performed using JADE 9.0 search/ matching and the powder diffraction file (PDF-4+) 2013 database from the International Center for Diffraction Data (ICDD). PDF numbers listed in the figures were taken from the ICDD database PDF-4 + . Slight non-stoichiometries in hydration or oxygen content can cause variations between reference lines reported for a given chemical species.

Isotopic verification. The uranium isotopic composition of the three samples (DU U_3O_8, NatU UO_3, HEU U_3O_8) was determined using a quadrupole inductively-coupled plasma mass spectrometer (Thermo X-series II ICP-MS equipped with a standard spray chamber). The DU U_3O_8 sample was received as a dissolved aliquot in 4 M nitric acid (HNO_3) at an approximate uranium concentration of 10 µg/mL. This sample was prepared for analysis using 2% HNO_3 for serial dilution. The NatU UO_3 and HEU U_3O_8 samples (~5 mg) were dissolved in separate operations using 3 M HNO_3, and then prepared for analysis after serial dilution using 2% HNO_3. Analytical acids were Optima grade and were prepared as stock reagents using 18.2 MΩ-cm (MilliQ) water.

Instrumental performance and mass bias corrections were determined using an analytical dilution of the Institute for Reference Materials and Measurements (IRMM) 74/1. Results are reported as uranium isotope atom percent composition (Table 1) and as atom ratios relative to U-235 (S1 Table in S1 File), with indicated measurement uncertainty representing 1-sigma standard deviation. Each sample was prepared and analyzed independently alongside an isotopically similar uranium standard to evaluate measurement quality. These data are presented along with the certified, or consensus, reference values for National Bureau of Standards Standard Reference Materials (SRMs) U-005, U-005A, U-960, and U-930 in S2 and S3 Tables in S1 File. The number of α-emissions per 24 hours per 100 µg of each uranium enrichment was calculated by multiplying the specific activity of each isotope at their respective isotopic composition percentage by the 100 µg sample to justify a significant difference of DU/NatU (1.24E + 05 and 2.24E + 05) α-radiation activity compared to our 90% U-235 enriched HEU (2.01E + 07).

Table 1. Isotopic analysis (percent) and estimation of α-emission rate of synthesized uranium oxide particulates. Uranium oxide samples were isotopically analyzed using a quadrupole inductively-coupled plasma mass spectrometer and compared to isotopically similar standardized uranium material. The α-emission rate of 100 µg of each sample for 24 hours was predicted by considering their isotopic composition and known specific activity of each isotope.

Sample ID	U-234	U-235	U-236	U-238	α-emissions/ 24 hours/ 100 µg
DU U_3O_8	0.000774(26)	0.2029(10)	0.00294(5)	99.793(1)	1.24E+05
NatU UO_3	0.005632(89)	0.7519(40)	0.000155(13)	99.242(3)	2.24E+05
HEU U_3O_8	0.9688(44)	90.754(39)	0.3476(18)	7.929(50)	2.01E+07

https://doi.org/10.1371/journal.pone.0334247.t001

Particulate sizing

Radiological and control particulate scanning electron microscopy (SEM) images were collected on a FEI Quanta 200F using field emission with accelerating voltages of 10–30 kV from gold-coated samples (Fig 1A). The optical diameters were established by dynamic light scattering (DLS) acquired with a Laser Scattering Particle Size Distribution Analyzer, Horiba LA-950 (Fig 1B). The size and morphology (shape factor, X) of TiO_2 and SiO_2 particulates were analyzed using established protocols of SEM, DLS, aerodynamic particulate sizing (APS), and optical particulate sizing (OPS) shown in Fig 1C using Eq. (1). Due to APS and OPS instruments being in a non-radiological space, the aerodynamic diameter of the uranium oxide particulates was theoretically calculated by the experimentally determined aerodynamic diameters of the non-radiological particulates.

$$D_{AE} = D_{IO}\sqrt{\frac{\rho_p}{\rho_0 X}}$$

(1)

D_{AE} is the theoretical aerodynamic particulate equivalent diameter, D_{IO} is the measured irregular particulate diameter found using DLS, ρ_B and ρ_0 are the bulk particulate density measured from the mass-to-volume ratio of loose powder and reference unit density of an example water droplet falling at terminal velocity ($\rho_0 = 1\,g/cm^3$), and X is the shape factor of the irregular particulate estimated by assessing the relative morphology of the particulates in the SEM images translating to literature values (Fig 1) [53]. All particulates showed a 3/2/1 cuboid shape factor (median = 1.745) except SiO_2, which showed a 3/2/1 ellipsoid (median = 1.36). Details of equivalent aerodynamic particulate diameters can be found in the supplemental information (S3 Fig, S4 and S5 Tables in S1 File). All particulates used for these experiments were shown in Table 2 to be respirable to humans (<10 µm MMAD).

Cell culture

Human adenocarcinoma lung epithelial cells, A549 (ATCC CL-185™), were cultured in tissue-treated T75 vented cap flasks (Corning®, 3290) with Ham's F-12 (Kaighn's Modification) with L-glutamine and without phenol red media (Caisson, HFL12) supplemented with 10% (v/v) Fetal Bovine Serum (FBS, F2442) from Sigma Aldrich at 37°C, 5% CO_2 in a humidified incubator (Benchmark Scientific, H3565-180). After 3 passages of reaching ~80% confluence, the A549s were seeded into a 96-well plate (Corning®, 3599) at 20,000 cells/well and incubated for 24 hours.

Primary human bronchial/tracheal epithelial cells (HBTEC, FC-0035, LOT #08265, LifeLine Cell Technologies®) and primary human small airway epithelial cells (HSAEC, FC-0016, LOT# 01434, LifeLine Cell Technologies®) were selected from healthy human donor lots. Each cell line was grown in T75 vented cap flasks (Corning®, 3290) with Lifeline® BronchiaLife™ Epithelial Airway Medium with Life Factors till ~80% confluence by changing the media every other day. The cells were then expanded in T175 cm² vented cap flasks (Corning®, CLS3292-50EA) again till ~80% confluence and cryopreserved. After 3–5 passages from the original manufactured vial, the cells were then seeded in a 96-well plate (Corning CellBIND®, 3300) at 40,000 cells/well and incubated for 3 days, changing the media every day.
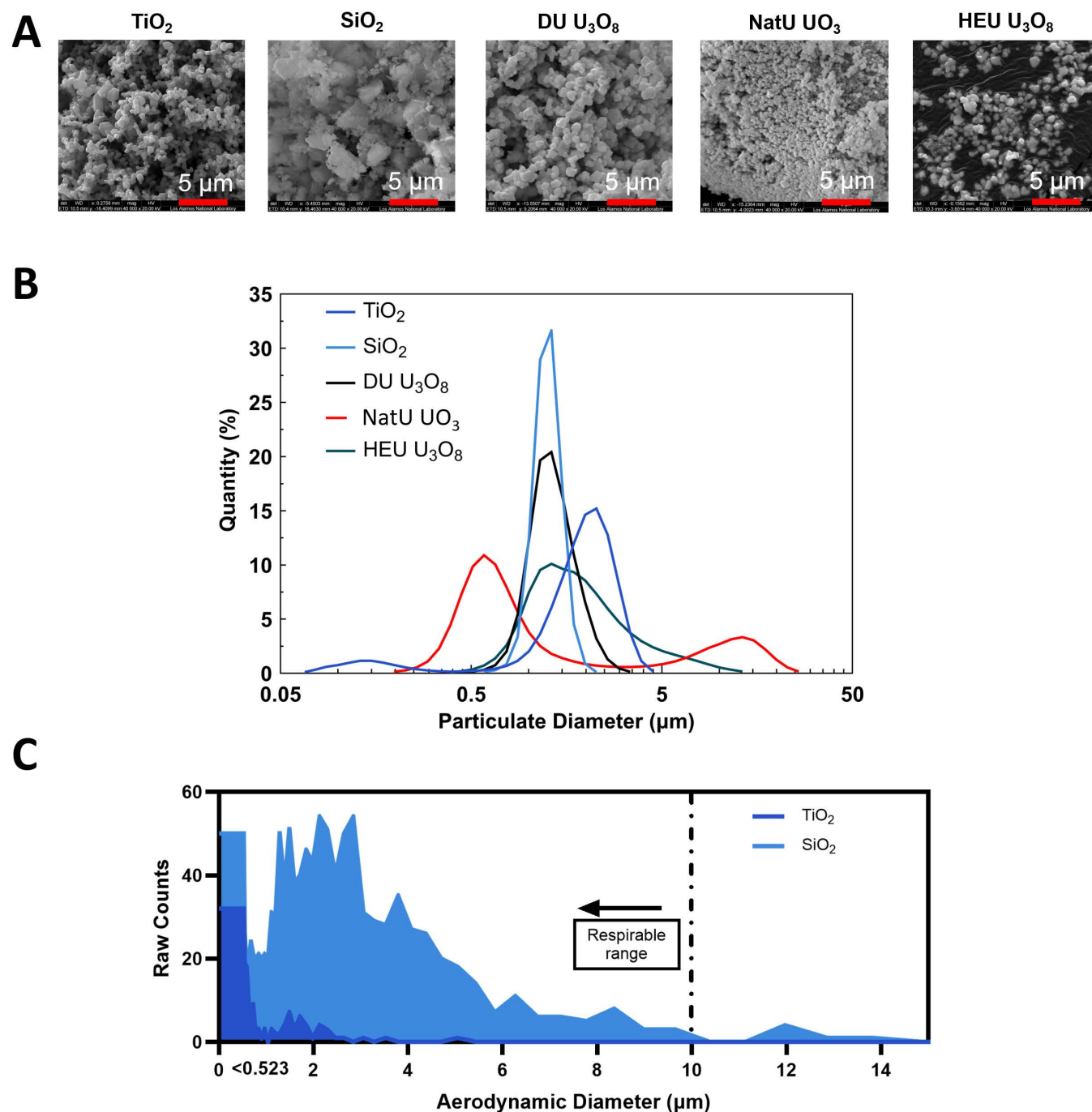
Fig 1. Characterization of particulates to calculate theoretical aerodynamic particulate size. (A) SEM images of all particulates for shape factor (X) estimation with a red scale bar of 5 μm. **(B)** DLS analysis of hydrodynamic diameter of all particulates shows majority within the human respirable range, < 10 μm MMAD. Dark blue = TiO_2, light blue = SiO_2, black = DU U_3O_8, red = NatU UO_3, and green = HEU U_3O_8. **(C)** Experimental aerodynamic particulate size of TiO_2 and SiO_2 to compare theoretical results.

https://doi.org/10.1371/journal.pone.0334247.g001

Table 2. Determination of aerodynamic equivalent particulate diameters through theoretical estimation. Radiological particulate aerodynamic equivalent diameters (D_{AE}) were theoretically estimated using experimentally determined irregular aerodynamic diameters (D_{IA}) of non-radiological particulates, TiO_2 and SiO_2, along with DLS irregular optical diameters (D_{IO}), bulk densities (ρ_B), and SEM-derived shape factors (*X*) from all respective particulates, and the reference density of water (ρ_0) with Eq. (1).

	Aerodynamic diameters, D_{IA}		Optical diameter sizes, D_{IO}					
Quantity	TiO_2	SiO_2	TiO_2	SiO_2	DU U_3O_8	NatU UO_3	HEU U_3O_8	
D_{IO} (µm)	1.54	2.08	1.828	1.173	1.224	0.802	1.583	Measured irregular particulate diameters
ρ_B (g/cm³)	0.77	2.32	0.77	2.32	8.3	8.3	8.3	Bulk powder density
ρ_0 (g/cm³)	1	1	1	1	1	1	1	Reference density
χ, unitless	1.745	1.36	1.745	1.36	1.745	1.745	1.745	Shape factor from online source [53]
D_{AE} (µm)	1.02	2.72	1.21	1.53	2.67	1.75	3.45	Aerodynamic equivalent diameter

https://doi.org/10.1371/journal.pone.0334247.t002

Cell viability and damage analysis

200 µL of varying concentrations of pre-sonicated (~20 minutes) uranium oxide and control particulates were added to each cell line. The particulate concentrations were 0.1, 1, 10, 50, 100, and 500 µg/mL. Cells were exposed to particulates in triplicate in each experiment, and each experiment was repeated four times for a total of 12 replicates. A positive cell damage control of 0.03% H_2O_2 was implemented, as well as an untreated cell negative control group.

The cell viability of each cell line was assessed by using water-soluble tetrazolium salt (WST-8) (Sigma Aldrich, 92992) and lactate dehydrogenase (LDH) activity assays (Sigma Aldrich, MAK066-1KT) using a plate reader (BioTek Synergy HTX). To assess a potential mechanism of cell death, a superoxide dismutase (SOD) assay (Sigma Aldrich, CS0009-1KT) was performed according to kit instructions, except for a 1:2 phosphate buffer saline (PBS) dilution of SOD product in each well before being read in the plate reader (BioTek Synergy HTX).

Statistical analysis

Due to the smaller sample size (n = 4), the statistical differences in cellular response were determined using the Mann-Whitney non-parametric test. The adjusted p-value was determined with the Bonferroni-Dunn method. Statistical relevance was determined by having a p-value less than 0.05 and was further categorized by <0.01, <0.001, and <0.0001 p-values, respectively. The degree of variance in each biological replicate (n = 4) was similar to the variance of total technical replicates (N = 12), allowing for the assumption to treat each of the 12 replicates for each particulate exposure as individual observations applied to the Mann-Whitney non-parametric test. For statistical comparison, the Mann-Whitney test results were compared to unmatched t-tests with a Welch correction using the Holm-Sidak method and showed no difference to the non-parametric test. Graphs were designed in GraphPad Prism v.10, and illustrations were designed in BioRender.

Ethics statement

The Los Alamos National Laboratory Human Subjects Research Review Board conducted an administrative review of the project prior to work and did not require a full review or assign a study number because the work was not considered human research. The NIH Human Subjects Research Decision Tool result of this study was "not considered human subjects research" since all specimens and data were obtained from deceased individuals.

Results

Toxicity assessment (LC(50)) in lung cells exposed to uranium oxides

Each of the cell lines tested, A549, HBTEC, and HSAEC, displayed dose dependent toxicity when exposed to different uranium oxide isotopes. Lethal concentrations for 50% cell death (LC(50)) curves demonstrate the impact of increasing

concentrations of uranium oxide on each type of cell, as compared to surrogate material ([Fig 2] and S4 Fig in [S1 File]). The LC(50) value was determined by plotting the normalized absorbance against uranium oxide concentration and fitting a sigmoidal curve. Lower LC(50) values demonstrate a greater cytotoxic effect of the uranium oxides on the cells. A549s demonstrated the lowest LC(50) of 169.5 µg/mL following exposure to DU U_3O_8, while HBTEC and HSAEC showed higher values of 949.1 µg/mL and 802.1 µg/mL, respectfully. LC(50) associated with NatU UO_3 indicates that A549 are most susceptible to changes in metabolism (110.0 µg/mL), followed by HSAEC (250.1 µg/mL) and HBTEC (364.6 µg/mL). We hypothesized that HEU U_3O_8 would have the smallest LC(50) amongst the different isotopes due to its increased α-radiation activity, thereby causing more cellular damage. This hypothesis was confirmed in the primary cell lines HBTEC (107.4 µg/mL) and HSAEC (225.5 µg/mL). A549s showed greater resilience to HEU U_3O_8 with an LC(50) value at
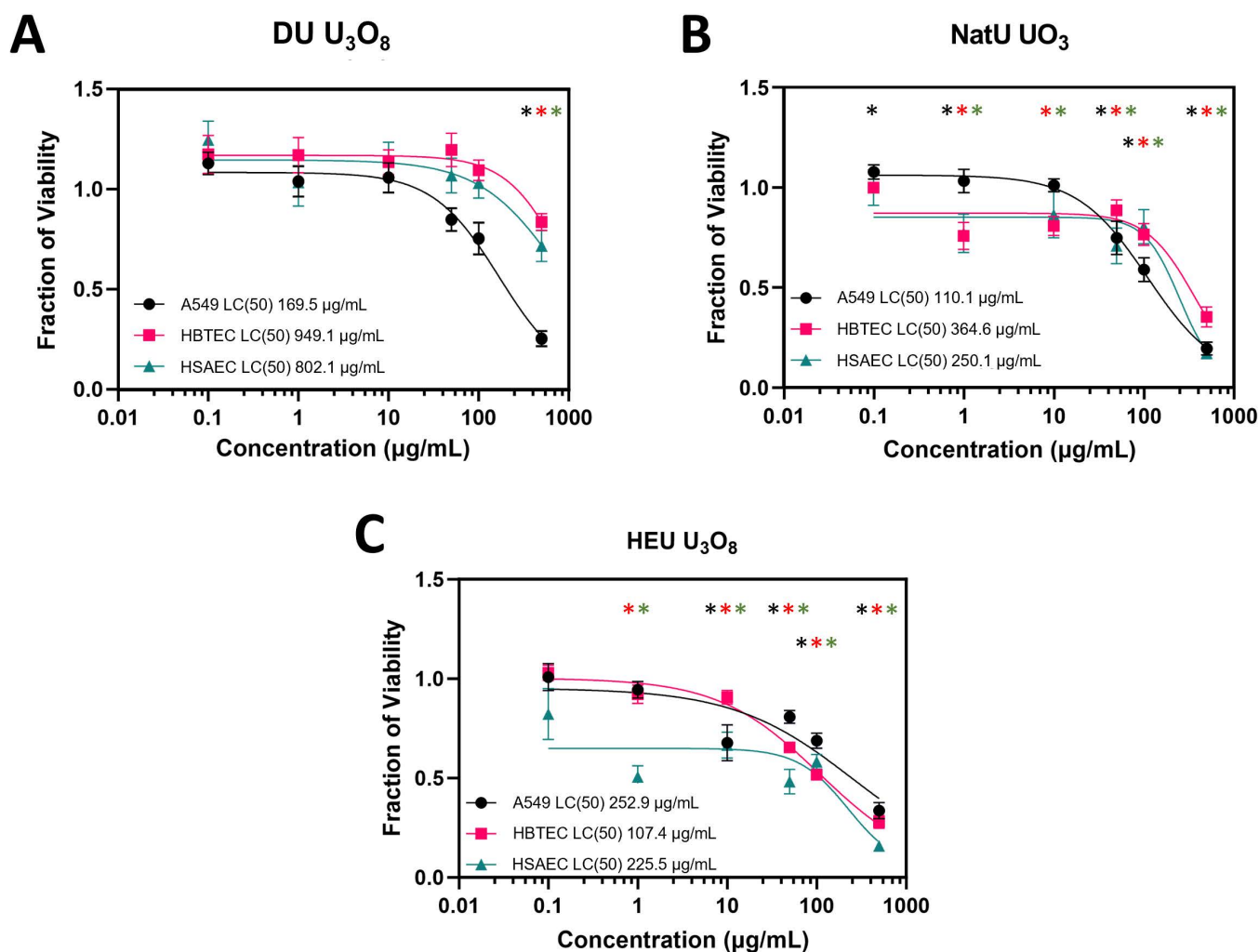

Fig 2. LC(50) curves of the effects of uranium particulates at differing enrichment values on A549, HBTEC, and HSAEC. WST-8 assay: **(A)** LC(50) of DU U_3O_8 on A549 (169.5 µg/mL), HBTEC (949.1 µg/mL), and HSAEC (802.1 µg/mL). **(B)** LC(50) of NatU UO_3 on A549 (110.0 µg/mL), HBTEC (364.6 µg/mL), and HSAEC (250.1 µg/mL). **(C)** LC(50) of HEU U_3O_8 on A549 (252.9 µg/mL), HBTEC (107.4 µg/mL), and HSAEC (225.5 µg/mL). All values after 24-hour exposure. Black = A549, red = HBTEC, and green = HSAEC. Colored asterisks (*) above data points indicate a significant fraction of viability ($p < 0.05$) compared to normalized untreated cells (fraction of viability = 1.0) respective of each cell line; biological replicates, n = 4 and technical replicate total, N = 12 for each condition.

https://doi.org/10.1371/journal.pone.0334247.g002

252.9 µg/mL. Thus, biological outcomes in immortalized cell lines vary from primary ones and may not be truly reflective of physiological systems.

Assessment of biological impact. 100 and 500 µg/mL of uranium oxide were selected for comprehensive bioanalysis because, based on the LC(50) values reported in Fig 2. All cell lines showed susceptibility to radioactive particulates at 500 µg/mL. At both 100 and 500 µg/mL, HBTEC and HSAEC demonstrated significantly increased cytotoxicity when compared to the untreated groups (Fig 3D), with both NatU UO_3 and HEU U_3O_8. At 100 µg/mL, these two cell lines did not demonstrate susceptibility to DU U_3O_8 particulates. Of cells exposed to 100 µg/mL of NatU UO_3 only HBTEC showed increased cytotoxicity (S5 Fig in S1 File). With exposure to 100 and 500 µg/mL of DU U_3O_8 particulates, A549 demonstrated the most significant decrease in viability ($p < 0.001$). No concentration dependence was measured in this cell line, and significant cytotoxic effects were observed in all exposure conditions compared to the untreated group (Fig 3C and 3D).

Lactate dehydrogenase (LDH) activity was measured in the cell lines following exposure to uranium oxides as an indication of reduced cell membrane integrity in response to the emitted radiation and physiochemical properties of the particulates. LDH are intracellular enzymes that leak out of the cell once the membrane is compromised and can be detected to assess the severity of cellular damage [54]. A dose-dependent response was observed, indicating that higher concentrations of uranium oxide particulates compromised cell membrane integrity, a key indicator of apoptosis and viability (S7 Fig in S1 File). At 100 and 500 µg/mL of all particulates, LDH activity in both HBTEC and HSAEC was significantly higher ($p < 0.01$) than in A549s (Fig 4A and 4B). HBTEC and HSAEC did not demonstrate significant differences between themselves. In the A549s, LDH activity was not significantly enhanced with either concentration of uranium (Fig 4C and 4D). LDH activity was significantly higher in primary cells exposed to DU U_3O_8 than in either NatU UO_3 or HEU U_3O_8. The one exception to this was HSAECs exposed to HEU U_3O_8 (Fig 4C and 4D).

Superoxide dismutases (SODs) are protective antioxidant enzymes that are essential in the defense against reactive oxygen species (ROS) produced by ionizing radiation or cellular processes [55]. We measured SOD activity in the cell lines following exposure to uranium oxides as an indication of a protective response to radiation exposure.

HBTECs showed the highest SOD activity when exposed to any of the particulates and at either concentration, while A549s had the lowest (Fig 5). All cell lines exhibited increased SOD activity when exposed to DU U_3O_8 and NatU UO_3, except A549s when exposed to 500 µg/mL of DU U_3O_8. HEU U_3O_8 did not induce a significant response in A549 and HSAEC, except when the latter was exposed at 500 µg/mL concentration (Fig 5C and 5D).

Discussion

Biological systems are extremely complex, and cell systems do not often effectively replicate this physiology. *In vitro* cultured cells respond differently to particulates based on type of cell, type of particulate, other factors such as oxidation state, and concentrations. Understanding the factors that contribute to the variability in cellular response to particulates can allow us to develop or integrate physiologically relevant *in vitro* models, which is our goal. In this manuscript, we begin to address this challenge via the simultaneous and systematic comparison of the response to distinctive uranium particulate enrichments (DU, NatU, and HEU) across varied lung cell (A549, HBTEC, and HSAEC). We assessed cell viability, health, and response over 24 hours via measurement of WST-8, LDH, and SOD activities in these cells. While our results reaffirmed that there is a significant difference in the response of different cells to uranium oxide particulates based on the type of enrichment, concentration, and oxide state, it also shed some light on the mechanisms and processes involved in these differences. Our outcomes strongly indicate the differences in the response between primary and immortalized cell lines, suggesting that the choice of the cell line should be carefully made, and mechanistic insights are required to evaluate the relevance of these differences in the physiological context. Thus, the continued systematic study of cell and tissue behavior in the context of radiological exposure is needed in order to provide data for toxicological analyses benchmarking their responses to *in vivo* human or animal data. Modern improvements of data availability and artificial intelligence
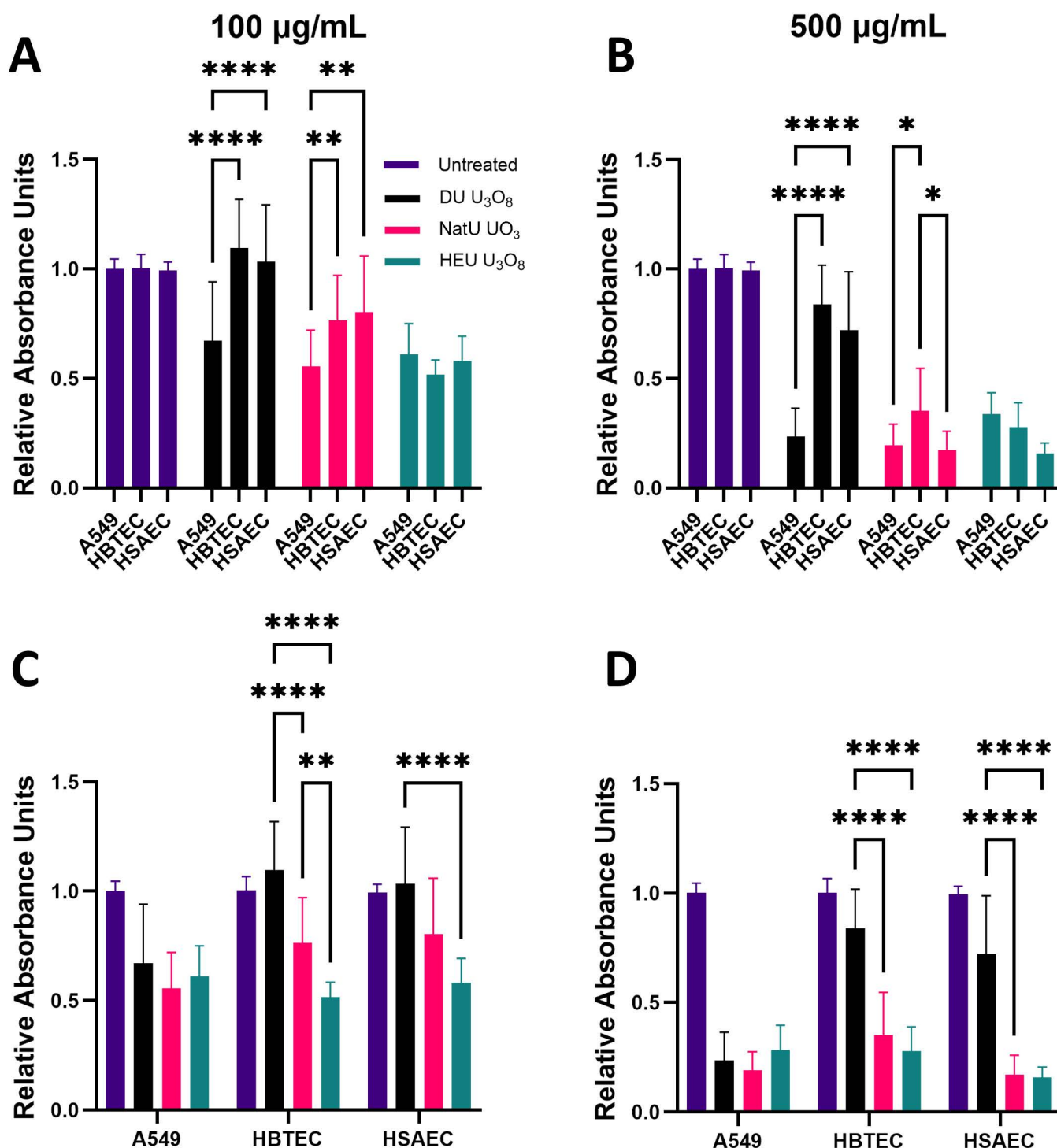
Fig 3. Assessing cell viability with WST-8 assay. Normalized A549, HBTEC, and HSAEC were exposed to 100 and 500 µg/mL of DU U_3O_8 (black), NatU UO_3 (red), and HEU U_3O_8 (green) for 24 hours. Normalized viability differences between cell lines exposed to (A) 100 µg/mL and (B) 500 µg/mL of uranium oxide particulates; A549 shows significantly decreased viability compared to HBTEC (p = 0.0047) and HSAEC (p = 0.0026) at 100 µg/mL. HBTEC and HSAEC showed significantly decreased normalized viability with exposure to NatU UO_3 (p < 0.0001) and HEU U_3O_8 (p < 0.0001) ((C) 100 µg/mL and (D) 500 µg/mL), compared to DU U_3O_8. An asterisk (*) indicates a significant fraction of viability: * (p < 0.05); ** (p < 0.01); *** (p < 0.001); **** (p < 0.0001) compared to normalized untreated cells (fraction of viability = 1.0); biological replicates, n = 4 and technical replicate total, N = 12 for each condition.

https://doi.org/10.1371/journal.pone.0334247.g003
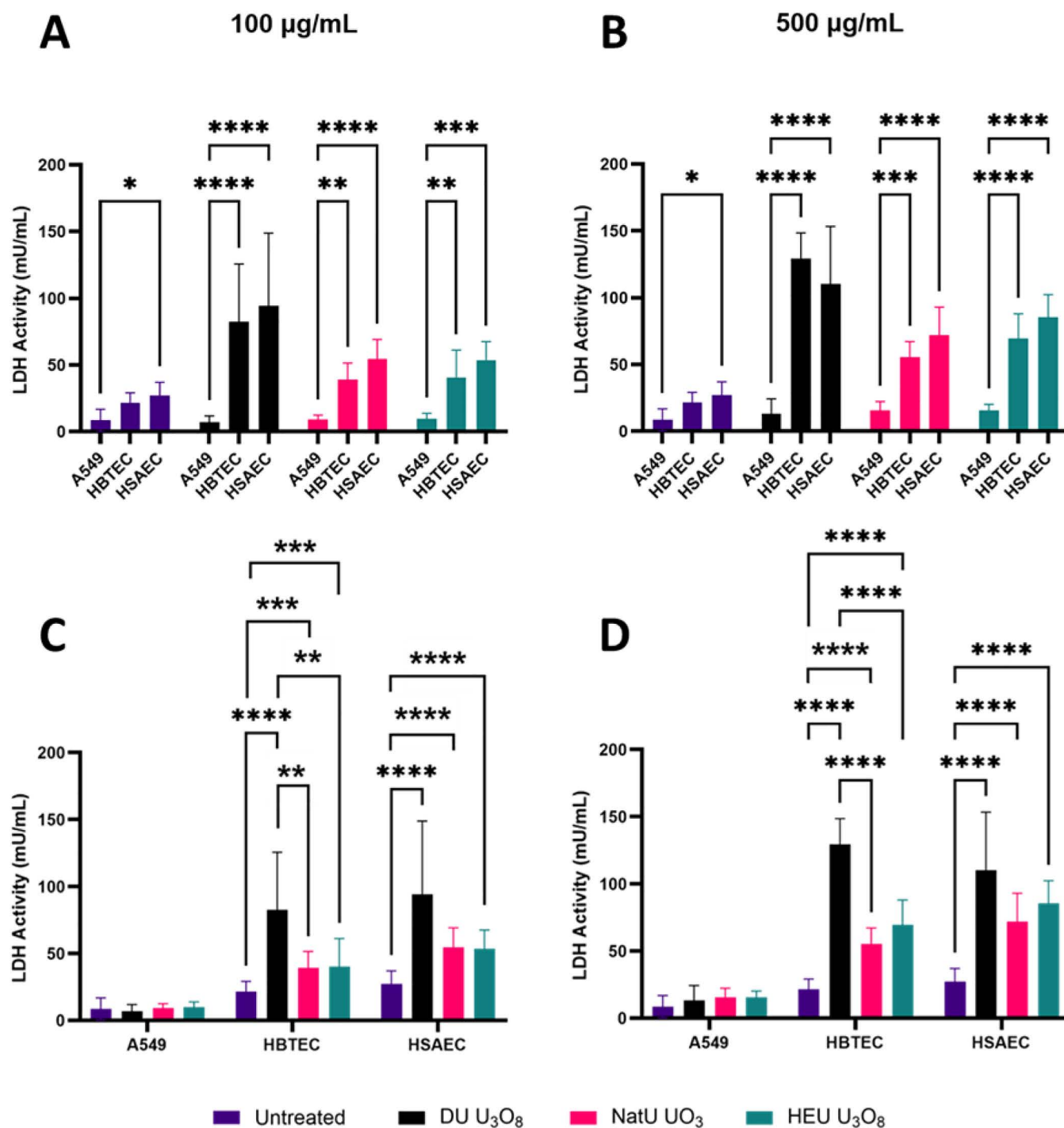
Fig 4. Measurement of LDH activity. LDH activity with 100 and 500 µg/mL of DU U_3O_8 (black), NatU UO_3 (red), and HEU U_3O_8 (green) for 24 hours in A549, HBTEC, and HSAEC. Statistical differences were observed with (A) 100 µg/mL and (B) 500 µg/mL of uranium oxide particulates; A549 consistently showed lower LDH activity compared to HBTEC ($p < 0.0001$) and HSAEC ($p < 0.0001$). LDH activity was statistically different for each cell line after (C) 100 µg/mL and (D) 500 µg/mL of uranium exposure; A549 showed no relative changes in LDH activity, while both HBTEC and HSAEC showed increased LDH activity to all uranium oxide particulates. An asterisk (*) indicates a significant fraction of viability: * ($p < 0.05$); ** ($p < 0.01$); *** ($p < 0.001$); **** ($p < 0.0001$) compared to normalized untreated cells (fraction of viability = 1.0); biological replicates, n = 4 and technical replicate total, N = 12 for each condition.

https://doi.org/10.1371/journal.pone.0334247.g004
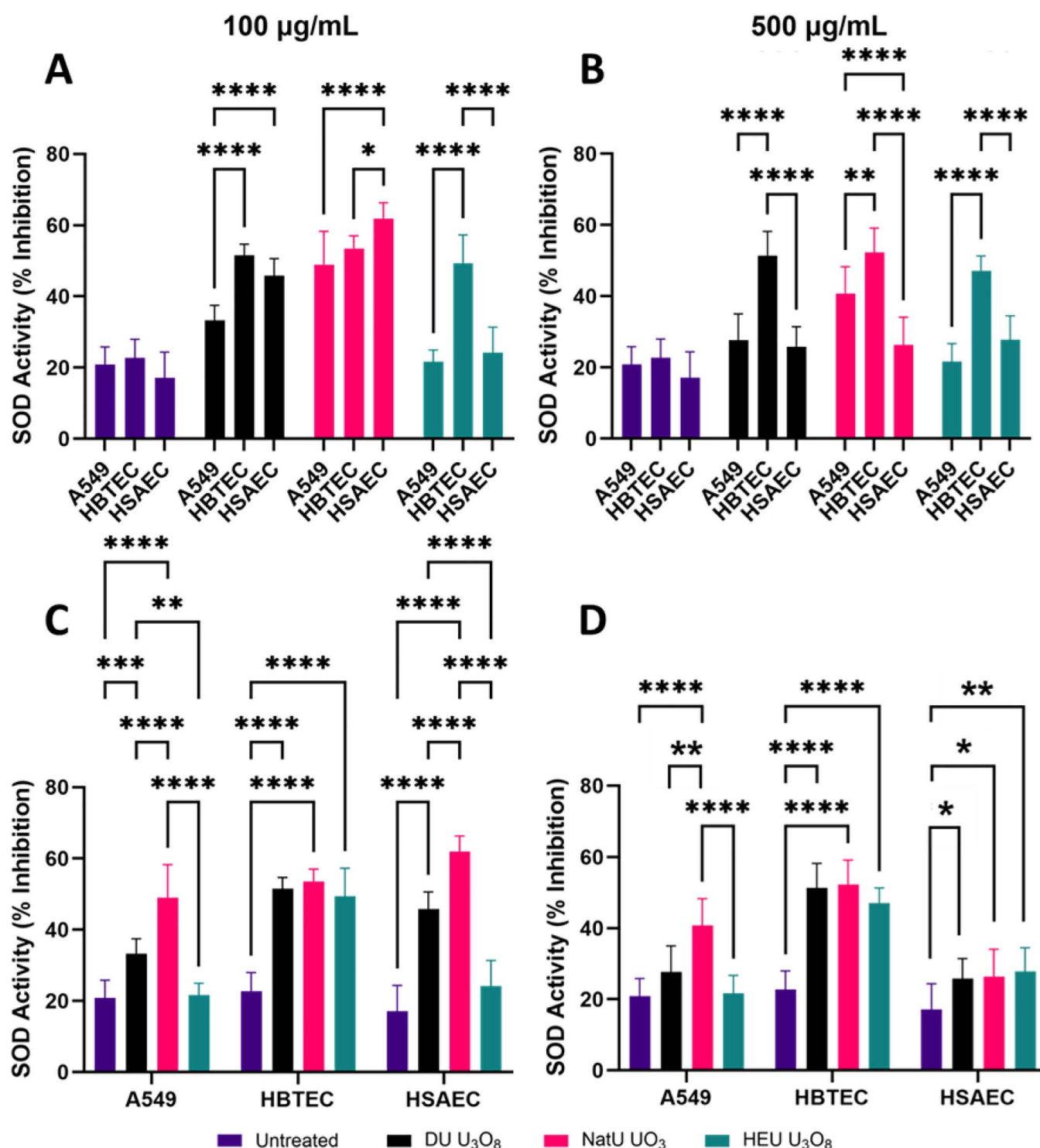
Fig 5. Measurement of SOD activity. SOD activity in A549, HBTEC, and HSAEC exposed to 100 and 500 μg/mL of DU U$_3$O$_8$ (black), NatU UO$_3$ (red), and HEU U$_3$O$_8$ (green) for 24 hours. (A) 100 μg/mL and (B) 500 μg/mL exposures to uranium oxides resulted in statistically significant induction of SOD activity. SOD activity with uranium oxide particulates for each cell line at (C) 100 μg/mL and (D) 500 μg/mL. An asterisk (*) indicates a significant change in SOD release: * ($p < 0.05$); ** ($p < 0.01$); *** ($p < 0.001$); **** ($p < 0.0001$) compared to normalized untreated cells (fraction of viability = 1.0); biological replicates, n = 4 and technical replicate total, N = 12 for each condition.

https://doi.org/10.1371/journal.pone.0334247.g005

(AI) models allow complex insights and detailed comparisons to translate results from *in vitro* to more physiologically relevant *in vivo* exposures, for instance accidental human exposures and animal studies [56]. AI models could tackle the fundamental challenge to extrapolate simplified *in vitro* models to more complicated *in vivo* models by accounting for the missing biological components presented in a whole organism and better understand dose responses. Our hope is that the *in vitro* results provided would be an initial step for these advanced AI comparisons to improve radiation protection strategies and risk assessments.

General viability of all cell lines was inhibited at some capacity in response to each of the uranium oxide particulates tested, and this response was concentration dependent as well. The U_3O_8 particulates had low (DU) and high (HEU) isotopic ratio samples to understand the effects of increasing α-radiation activity on cells. Exposure to HEU U_3O_8 particulates significantly decreased HBTEC and HSAEC viability and proliferation compared to DU U_3O_8, as measured by the WST-8 cells (Fig 3). Conversely, A549s were sensitive to both DU and HEU U_3O_8 particulates, but the increased isotopic ratios did not magnify toxicity, as the measurements were not statistically different under these two exposure conditions. Since A549s demonstrated equal toxicity to all tested isotopic contents, it is probable that they are more sensitive to the uranium particulates—that is, *via* chemical properties than radiological toxicity—but further testing is required to justify this claim. The reduced response of primary cell lines to DU could potentially be due to their more stabilized genome, which may contribute to protection against radiological insult and/or heavy metal toxicity [57]. In addition, the differences between immortalized and primary cells in cell death and repair gene expression may account for some of the differences seen in the current study [58]. The number of cellular passages can also affect phenotypic results and genes related to the cell cycle that are expressed [59].

The fissile U-235 content of natural UO_3 (0.7519%) is not dramatically different from that of depleted U_3O_8 (0.2029%). Thus, α-radiation activity over 24 hours is relatively similar in both samples (Table 1). UO_3 has a greater number of moles per gram of uranium than U_3O_8. This is accounted for in the emissions calculations for Table 1. However, viability and proliferation when exposed to NatU UO_3 were consistently lower as compared to the DU U_3O_8, a result especially seen in the primary cell lines. This may be associated with the comparatively higher presence of U-234 with its high-energy daughters, enhanced solubility, and consequent bioavailability of the isotope. UO_3 and U_3O_8 are mostly insoluble in water, but UO_3 solubility has been observed to be greatly enhanced in solutions with inorganic salts, such as NaCl, KCl, and KNO_3, suggesting higher solubility in cell media [32,60]. The soluble form of UO_3, uranyl hydroxide ($UO_2(OH)_2$), can potentially cause more robust internal damage due to its ionic complexation with cell membrane permeable proteins [61]. Thus, the oxidation state of uranium particulates could modulate toxicological responses based on their solubility even at 24 hours of exposure. A systematic study of toxicology as a function of particulate solubility can help derive more robust inferences.

In assessing cellular respiration via LDH activity, no increase was evidenced in A549s for any of the uranium oxides, even though significant enhancement was noted in the primary cell models. The physiological makeup of immortalized versus primary cell lines results in disparate outcomes in such studies and must be better characterized to ensure relevance. LDH activities following exposure to depleted U_3O_8 were significantly higher for both primary cell lines compared to those associated with NatU UO_3 and HEU U_3O_8. Whereas this could be truly indicative of the biological interactions being assessed, it is important to rule out artifactual factors such as the influence of media composition, among others. For instance, the media used for primary cell cultures is serum-free and produced a small amount of precipitate when the uranium particulates were added, whereas the A549 serum-containing media showed no sign of complexation. Controls, such as PBS with uranium oxides and both serum and serum-free cell media with uranium oxides without cells, were implemented to account for the possibility that the formed precipitate produced scattering of the plate reader laser and skewed the absorbance values. We subtracted values from wells that contained only uranium oxides and serum-free media, but it is uncertain whether the additional cell interaction with the oxides magnified scattering of the beam. A possible explanation for the formation of the precipitate is that the ionic form of the uranium oxides, uranyl (UO_2^{2+}), complexed with the anionic species present in the serum-free primary media. Specific fats and proteins from the A549 serum-containing media could

have interrupted any uranium precipitates from forming. Further investigation into this speciation of uranium in serum- and non-serum-containing media—as well as common cell culture additives like antibiotics—is currently ongoing in our laboratory by using ultraviolet and Raman spectroscopy to identify the components that contribute to precipitation. By comparing the Raman spectra of serum and serum-free media with uranium oxide, a molecular fingerprint can be identified. Another possibility is that the LDH release was inactivated by certain unknown reactive chemicals in the A549 media or mixture of media with the uranium particulates, causing low levels of LDH [62]. The addition of 10% FBS to the A549 media is known to show increased LDH levels, which is contradictory to what was seen in the results [63]. The cellular mechanisms as to why DU U_3O_8 significantly increased LDH activity compared to HEU U_3O_8 in primary cells are notable and will be investigated in future projects.

SOD activity generally increased across all cell models and uranium oxides compared to untreated controls. Upon exposure to HEU U_3O_8, HBTECs showed significantly elevated SOD activity compared to either A549 or HSAEC models. This is one of the few cases wherein a difference in activity was observed among the primary cell types. HBTECs were the only cell model that expressed significantly elevated SOD activity to each uranium oxide particulate at 100 and 500 µg/mL. At 100 µg/ml, no SOD activity was evidenced in HEU U_3O_8, which did not elicit an increase in SOD activity in A549 or HSAEC, indicating that it takes a more significant exposure risk to induce protective mechanisms in these *in vitro* models. The mechanism as to why DU U_3O_8 was able to cause increased SOD activity compared to HEU U_3O_8 in the smaller airway cell models may relate to higher SOD response as a protective mechanism in the upper airway [64].

Conclusions

Our studies begin to shed light on mechanistic insights into the properties of cell-based systems and their suitability for studying exposure to uranium particulates. Each cell line responded differently to uranium particulates, further influenced by enrichment or oxidation state. Variations in oxidation states of the uranium particulates influenced viability across all cell lines, whereas increased enrichment corresponded to increased toxicity in the primary cells, HBTEC and HSAEC, but not for the immortalized A549. Primary upper respiratory tract cells, HBTEC, displayed decreased viability and increased SOD activity levels, correlating with the greatest general susceptibility to all radioactive particulates (DU U_3O_8, NatU UO_3, and HEU U_3O_8). These findings indicate that a comprehensive assessment of cell system viability and the influence of underlying factors (media composition, stage of growth, confluence, type of particulate) is required before deeper conclusions on the impact to complex biosystems can be drawn from cell studies. However, with modern improvements of data availability and artificial intelligence models, these *in vitro* results can potentially be translated/compared to more physiologically relevant *in* vivo human exposures, alongside animal studies, to advance radiation protection strategies risk assessments, and countermeasure development. Future directions include the further disassociation of α-radiation from heavy-metal particulate toxicity to understand which mechanism is the underlying, or greater, cause of cellular death. Finally, systematic time-course evaluations to investigate prolonged dose response and investigations of the solubilities of different uranium oxides in cell media and the complexes they produce will be needed to create additional data sets that can be applied to translational toxicology studies in understanding how these cell types relate to human response.

Supporting information

S1 File. Characterization of particulates and additional controls.
(DOCX)

S1 Fig. Graphical abstract—Overview of the study design. Three different enrichment states and two oxide states of uranium particulates were separately introduced to three distinct submerged *in vitro* human epithelial lung cell lines to investigate if increased alpha emissions, oxidation state, or respiratory tract location causes differences in toxicological effect.
(TIF)

Acknowledgments

Author contributions

Conceptualization: Harshini Mukundan, Jennifer Foster Harris.

Data curation: Shepard C. Moore, Warren J. Oldham.

Formal analysis: Gregory L. Wagner, Warren J. Oldham.

Funding acquisition: Harshini Mukundan, Jennifer Foster Harris.

Investigation: Shepard C. Moore, Laura M. Lilley, Julie Strickland, Mohammad Omar Ishak, William Conor Emberley, Brian L. Scott, Gregory L. Wagner, Warren J. Oldham, Murray E. Moore.

Methodology: Laura M. Lilley, Julie Strickland, Mohammad Omar Ishak, William Conor Emberley, Gregory L. Wagner, Warren J. Oldham, Murray E. Moore, Harshini Mukundan.

Resources: Gregory L. Wagner.

Supervision: Laura M. Lilley, Gregory L. Wagner, Harshini Mukundan, Jennifer Foster Harris.

Validation: Shepard C. Moore.

Visualization: Laura M. Lilley, Warren J. Oldham.

Writing – original draft: Shepard C. Moore.

Writing – review & editing: Laura M. Lilley, Gregory L. Wagner, Murray E. Moore, Harshini Mukundan, Jennifer Foster Harris.

References

1. Radiation UNSCotEoA. Sources, Effects and Risks of Ionizing Radiation, United Nations Scientific Committee on the Effects of Atomic Radiation (UNSCEAR) 2016 Report. United Nations; 2017.

2. Keith S, Faroon O, Roney N, Scinicariello F, Wilbur S, Ingerman L, et al. Agency for Toxic Substances and Disease Registry (ATSDR) Toxicological Profiles. Toxicological Profile for Uranium. Atlanta (GA): Agency for Toxic Substances and Disease Registry (US); 2013.

3. Gao N, Huang Z, Liu H, Hou J, Liu X. Advances on the toxicity of uranium to different organisms. Chemosphere. 2019;237:124548. https://doi.org/10.1016/j.chemosphere.2019.124548 PMID: 31549660

4. Bolt HM. The Janus face of uranium in toxicology. Arch Toxicol. 2022;96(3):689–90. https://doi.org/10.1007/s00204-022-03223-3 PMID: 35118510

5. Ran Y, Wang S, Zhao Y, Li J, Ran X, Hao Y. A review of biological effects and treatments of inhaled depleted uranium aerosol. J Environ Radioact. 2020;222:106357. https://doi.org/10.1016/j.jenvrad.2020.106357 PMID: 32755761

6. Giuranno L, Ient J, De Ruysscher D, Vooijs MA. Radiation-Induced Lung Injury (RILI). Front Oncol. 2019;9:877. https://doi.org/10.3389/fonc.2019.00877 PMID: 31555602

7. Chauhan V, Howland M, Kutzner B, McNamee JP, Bellier PV, Wilkins RC. Biological effects of alpha particle radiation exposure on human mono-cytic cells. Int J Hyg Environ Health. 2012;215(3):339–44. https://doi.org/10.1016/j.ijheh.2011.11.002 PMID: 22153871

8. Bannik K, Madas B, Jarzombek M, Sutter A, Siemeister G, Mumberg D, et al. Radiobiological effects of the alpha emitter Ra-223 on tumor cells. Sci Rep. 2019;9(1):18489. https://doi.org/10.1038/s41598-019-54884-7 PMID: 31811257

9. Dornish M, Heier-Baardson H, Pettersen E. Cellular effects of alpha particle radiation from radium-223: Alpharadin™, a new radiopharmaceutical for the treatment of skeletal metastases. Cancer Res. 2008;68(9_Supplement):5749.

10. Chauhan V, Howland M, Mendenhall A, O'Hara S, Stocki TJ, McNamee JP, et al. Effects of alpha particle radiation on gene expression in human pulmonary epithelial cells. Int J Hyg Environ Health. 2012;215(5):522–35. https://doi.org/10.1016/j.ijheh.2012.04.004 PMID: 22608759

11. Nojima H, Kaida A, Matsuya Y, Uo M, Yoshimura R-I, Arazi L, et al. DNA damage response in a 2D-culture model by diffusing alpha-emitters radiation therapy (Alpha-DaRT). Sci Rep. 2024;14(1):11468. https://doi.org/10.1038/s41598-024-62071-6 PMID: 38769339

12. Danforth JM, Provencher L, Goodarzi AA. Chromatin and the Cellular Response to Particle Radiation-Induced Oxidative and Clustered DNA Damage. Front Cell Dev Biol. 2022;10:910440. https://doi.org/10.3389/fcell.2022.910440 PMID: 35912116

13. Azzam EI, Jay-Gerin J-P, Pain D. Ionizing radiation-induced metabolic oxidative stress and prolonged cell injury. Cancer Lett. 2012;327(1–2):48–60. https://doi.org/10.1016/j.canlet.2011.12.012 PMID: 22182453

14. Cohen–Jonathan E, Bernhard EJ, McKenna WG. How does radiation kill cells? Curr Opin Chem Biol. 1999;3(1):77–83.

15. Routes E, Food I, Radio L, Ground WB, Exposure E, Exposure I, et al. Various Forms of Exposure. 2018;1:23–75.

16. NuDat 3.0 [Internet]. National Nuclear Data Center; 2025. Available from: https://www.nndc.bnl.gov/nudat3/

17. Keith S, Faroon O, Roney N, et al. Toxicological Profile for Uranium: Agency for Toxic Substances and Disease Registry (US). Atlanta, GA; 2013.

18. Kathren RL, Burklin RK. Acute chemical toxicity of uranium. Health Phys. 2008;94(2):170–9. https://doi.org/10.1097/01.HP.0000288043.94908.1f PMID: 18188051

19. Ma M, Wang R, Xu L, Xu M, Liu S. Emerging health risks and underlying toxicological mechanisms of uranium contamination: Lessons from the past two decades. Environ Int. 2020;145:106107. https://doi.org/10.1016/j.envint.2020.106107 PMID: 32932066

20. Oliver AJ, Özberk E. 11 - Conversion of natural uranium. In: Hore-Lacy I, editor. Uranium for Nuclear Power. Woodhead Publishing; 2016. p. 299–319.

21. Hore-Lacy I. 1 - Uranium for nuclear power: An introduction. In: Hore-Lacy I, editor. Uranium for Nuclear Power. Woodhead Publishing; 2016. p. 3–10.

22. Harding P. 12 - Uranium enrichment. In: Hore-Lacy I, editor. Uranium for Nuclear Power. Woodhead Publishing; 2016. p. 321–51.

23. Zhang L, Chu J, Xia B, Xiong Z, Zhang S, Tang W. Health Effects of Particulate Uranium Exposure. Toxics. 2022;10(10).

24. Ao B, Qiu R, Tang J, Chen J. New theoretical insights into the actual oxidation states of uranium in the solid-state compounds. J Nucl Mater. 2021;543:152563. https://doi.org/10.1016/j.jnucmat.2020.152563

25. Li P, Lu Z, Wang J, He T, Ou N, Liang J, et al. XPS determination of the uranium valences in U3O8. Nuclear Analysis. 2023;2(2):100071. https://doi.org/10.1016/j.nucana.2023.100071

26. Wilson HB, Sylvester GE, et al. The relation of particle size of uranium dioxide dust to toxicity following inhalation by animals; preliminary report. J Ind Hyg Toxicol. 1948;30(6):319–31. PMID: 18100363

27. Prat O, Berenguer F, Malard V, Tavan E, Sage N, Steinmetz G, et al. Transcriptomic and proteomic responses of human renal HEK293 cells to uranium toxicity. Proteomics. 2005;5(1):297–306. https://doi.org/10.1002/pmic.200400896 PMID: 15672453

28. Periyakaruppan A, Kumar F, Sarkar S, Sharma CS, Ramesh GT. Uranium induces oxidative stress in lung epithelial cells. Arch Toxicol. 2007;81(6):389–95. https://doi.org/10.1007/s00204-006-0167-0 PMID: 17124605

29. Harris WB, Davies E. Experimental clearance of uranium dust from the human body. Inhaled particles and vapours. London: Pergamon; 1961.

30. Kazzi Z, Buzzell J, Bertelli L, Christensen D. Emergency department management of patients internally contaminated with radioactive material. Emerg Med Clin North Am. 2015;33(1):179–96. https://doi.org/10.1016/j.emc.2014.09.008 PMID: 25455668

31. Fahy JV, Dickey BF. Airway mucus function and dysfunction. N Engl J Med. 2010;363(23):2233–47. https://doi.org/10.1056/NEJMra0910061 PMID: 21121836

32. Bolch WE, Jokisch D, Zankl M, Eckerman KF, Fell T, Manger R, et al. ICRP Publication 133: The ICRP computational framework for internal dose assessment for reference adults: specific absorbed fractions. Ann ICRP. 2016;45(2):5–73.

33. Sturm R. Radioactivity and lung cancer-mathematical models of radionuclide deposition in the human lungs. J Thorac Dis. 2011;3(4):231–43. https://doi.org/10.3978/j.issn.2072-1439.2011.04.01 PMID: 22263097

34. Hill RP. Radiation effects on the respiratory system. Br J Radiol. 2014;78(Supplement_27):75–81.

35. Anadón A, Martínez MA, Castellano V, Martínez-Larrañaga MR. The role of in vitro methods as alternatives to animals in toxicity testing. Expert Opin Drug Metab Toxicol. 2014;10(1):67–79. https://doi.org/10.1517/17425255.2014.854329 PMID: 24160258

36. El Hayek E, Medina S, Guo J, Noureddine A, Zychowski KE, Hunter R, et al. Uptake and Toxicity of Respirable Carbon-Rich Uranium-Bearing Particles: Insights into the Role of Particulates in Uranium Toxicity. Environ Sci Technol. 2021;55(14):9949–57. https://doi.org/10.1021/acs.est.1c01205 PMID: 34235927

37. Ohshima S, Xu Y, Takahama M. Effects of uranium ore dust on cultured human lung cells. Environ Toxicol Pharmacol. 1998;5(4):267–71. https://doi.org/10.1016/s1382-6689(98)00010-6 PMID: 21781873

38. Quevedo R, Smirnov P, Tkachuk D, Ho C, El-Hachem N, Safikhani Z, et al. Assessment of Genetic Drift in Large Pharmacogenomic Studies. Cell Systems. 2020;11(4):393–401.e2.

39. Werner AN, Kumar AI, Charest PG. CRISPR-mediated reversion of oncogenic KRAS mutation results in increased proliferation and reveals independent roles of Ras and mTORC2 in the migration of A549 lung cancer cells. Mol Biol Cell. 2023;34(13):ar128. https://doi.org/10.1091/mbc.E23-05-0152 PMID: 37729017

40. Richter M, Piwocka O, Musielak M, Piotrowski I, Suchorska WM, Trzeciak T. From Donor to the Lab: A Fascinating Journey of Primary Cell Lines. Front Cell Dev Biol. 2021;9:711381. https://doi.org/10.3389/fcell.2021.711381 PMID: 34395440

41. Hare D, Collins S, Cuddington B, Mossman K. The Importance of Physiologically Relevant Cell Lines for Studying Virus-Host Interactions. Viruses. 2016;8(11):297. https://doi.org/10.3390/v8110297 PMID: 27809273

42. Balharry D, Sexton K, BéruBé KA. An in vitro approach to assess the toxicity of inhaled tobacco smoke components: nicotine, cadmium, formaldehyde and urethane. Toxicology. 2008;244(1):66–76. https://doi.org/10.1016/j.tox.2007.11.001 PMID: 18082304

43. Nova Z, Skovierova H, Strnadel J, Halasova E, Calkovska A. Short-Term versus Long-Term Culture of A549 Cells for Evaluating the Effects of Lipopolysaccharide on Oxidative Stress, Surfactant Proteins and Cathelicidin LL-37. Int J Mol Sci. 2020;21(3):1148. https://doi.org/10.3390/ijms21031148 PMID: 32050475

44. Pan C, Kumar C, Bohl S, Klingmueller U, Mann M. Comparative proteomic phenotyping of cell lines and primary cells to assess preservation of cell type-specific functions. Mol Cell Proteomics. 2009;8(3):443–50. https://doi.org/10.1074/mcp.M800258-MCP200 PMID: 18952599

45. Van Norman GA. Limitations of Animal Studies for Predicting Toxicity in Clinical Trials: Is it Time to Rethink Our Current Approach? JACC Basic Transl Sci. 2019;4(7):845–54. https://doi.org/10.1016/j.jacbts.2019.10.008 PMID: 31998852

46. Atkins JT, George GC, Hess K, Marcelo-Lewis KL, Yuan Y, Borthakur G, et al. Pre-clinical animal models are poor predictors of human toxicities in phase 1 oncology clinical trials. Br J Cancer. 2020;123(10):1496–501. https://doi.org/10.1038/s41416-020-01033-x PMID: 32868897

47. Robinson NB, Krieger K, Khan FM, Huffman W, Chang M, Naik A, et al. The current state of animal models in research: A review. Int J Surg. 2019;72:9–13. https://doi.org/10.1016/j.ijsu.2019.10.015 PMID: 31627013

48. Carter M, Essner R, Goldstein N, Iyer M. Chapter 13 - Cell Culture Techniques. In: Carter M, Essner R, Goldstein N, Iyer M, editors. Guide to Research Techniques in Neuroscience. 3rd ed. Academic Press; 2022. p. 291–308.

49. Limits for intakes of radionuclides by workers ICRP publication 30, part 1, 1979. Ann ICRP. 1980;4(3–4):I–I. https://doi.org/10.1016/0146-6453(80)90046-9

50. Tamasi AL, Boland KS, Czerwinski K, Ellis JK, Kozimor SA, Martin RL, et al. Oxidation and hydration of U3O8 materials following controlled exposure to temperature and humidity. Anal Chem. 2015;87(8):4210–7. https://doi.org/10.1021/ac504105t PMID: 25786096

51. Mohan A, Moorthy VK. Solid solution formation in UO2-ThO2 system. Trans Indian Ceramic Soc. 1971;30(5):124–32.

52. Tomasi R. Study of the sintering process and the formation of a (Th, U) O 2 solid solution.

53. Saucier R. Shape Factor Modeling and Simulation. Army Research Lab; 2016.

54. Kaja S, Payne AJ, Naumchuk Y, Koulen P. Quantification of Lactate Dehydrogenase for Cell Viability Testing Using Cell Lines and Primary Cultured Astrocytes. Curr Protoc Toxicol. 2017;72:2.26.1-2.26.10. https://doi.org/10.1002/cptx.21 PMID: 28463416

55. Lee JH, Choi IY, Kil IS, Kim SY, Yang ES, Park JW. Protective role of superoxide dismutases against ionizing radiation in yeast. Biochim Biophys Acta. 2001;1526(2):191–8. https://doi.org/10.1016/s0304-4165(01)00126-x PMID: 11325541

56. Chandra M, Li T, Tong W. AIVIVE: a novel AI framework for enhanced in vitro to in vivo extrapolation (IVIVE) of toxicogenomics data. Toxicol Sci. 2025;207(2):361–71. https://doi.org/10.1093/toxsci/kfaf100 PMID: 40692113

57. Brezden CB, Rauth AM. Differential cell death in immortalized and non-immortalized cells at confluency. Oncogene. 1996;12(1):201–6. PMID: 8552393

58. Hellmann GM, Fields WR, Doolittle DJ. Gene expression profiling of cultured human bronchial epithelial and lung carcinoma cells. Toxicol Sci. 2001;61(1):154–63. https://doi.org/10.1093/toxsci/61.1.154 PMID: 11294986

59. Cooper JR, Abdullatif MB, Burnett EC, Kempsell KE, Conforti F, Tolley H, et al. Long Term Culture of the A549 Cancer Cell Line Promotes Multilamellar Body Formation and Differentiation towards an Alveolar Type II Pneumocyte Phenotype. PLoS One. 2016;11(10):e0164438. https://doi.org/10.1371/journal.pone.0164438 PMID: 27792742

60. Stuart WI, Adams RB, Smith HE. Solubility and hemolytic activity of uranium trioxide. Environ Res. 1979;18(2):385–96. https://doi.org/10.1016/0013-9351(79)90115-4 PMID: 41704

61. Benavides-Garcia MG, Balasubramanian K. Structural insights into the binding of uranyl with human serum protein apotransferrin structure and spectra of protein-uranyl interactions. Chem Res Toxicol. 2009;22(9):1613–21. https://doi.org/10.1021/tx900184r PMID: 19678663

62. Kendig DM, Tarloff JB. Inactivation of lactate dehydrogenase by several chemicals: implications for in vitro toxicology studies. Toxicol In Vitro. 2007;21(1):125–32. https://doi.org/10.1016/j.tiv.2006.08.004 PMID: 17079110

63. Thomas MG, Marwood RM, Parsons AE, Parsons RB. The effect of foetal bovine serum supplementation upon the lactate dehydrogenase cytotoxicity assay: Important considerations for in vitro toxicity analysis. Toxicol In Vitro. 2015;30(1 Pt B):300–8. https://doi.org/10.1016/j.tiv.2015.10.007 PMID: 26498060

64. Albano GD, Gagliardo RP, Montalbano AM, Profita M. Overview of the Mechanisms of Oxidative Stress: Impact in Inflammation of the Airway Diseases. Antioxidants (Basel). 2022;11(11):2237. https://doi.org/10.3390/antiox11112237 PMID: 36421423